# Numerical Modeling of Near Corona Wire Electrohydrodynamic Flow in a Wire-plate Electrostatic Precipitator

**Young Nam Chun**
BK 21 Team for Biohydrogen Production
Department of Environmental Engineering, Chosun University, Seosukdong, 501-759, Gwangju, R. Korea

**Jen-Shih Chang , Alexander A. Berezin**
Department of Engineering Physics, McMaster University, Hamilton, Ontario, L8S 4L7 Canada

and **J. Mizeraczyk**
Institute of Fluid Flow Machinery, Polish Academy of Sciences, Gdansk, Poland

## ABSTRACT

**Numerical modelling of the flow velocity fields for the near corona wire electrohydrodynamic (EHD) flow was conducted. Solutions of the steady, two-dimensional momentum equations have been computed for a wire-plate type electrostatic precipitator (ESP). The equations were solved in the conservative finite-difference form on a fine uniform rectilinear grid of sufficient resolution to accurately capture the momentum boundary layers. The numerical procedure for the differential equations was used by SIMPLEST [1] algorithm. The CFD code [2], coupled with Poisson's electric field, ion transport equations and the momentum equation with electric body force, was used for the numerical simulation with the Chen-Kim $k-\varepsilon$ turbulent model. The numerical results show that EHD secondary flow was clearly visible in the downstream regions of the corona wire despite the low Reynolds number for the electrode ($Re_{CW}$=12.4). Secondary flow vortices caused by the EHD increases with increasing discharge current or EHD number, hence pressure drop of ESP increases.**

Index Terms — **Electrodynamics, electrostatic precipitator, EHD turbulent modeling, Von-Karman type vortex.**

## 1 INTRODUCTION

**INDUSTRIAL** electrostatic precipitation (ESP) has a very complex interaction between the electric field, gas and particulate flow. The motion and precipitation of dust particles in an ESP depends on the electric field, space charge, gas flow field and dust particle properties.

The several investigations [3,4] that estimated EHD flow effects on the dust particle collections, may be significant. However, it is still unclear whether these EHD turbulent flow structures enhances or deteriorates fine particle precipitation processes. EHD turbulence can be generated, even for Reynolds number less than 1, if the EHD number (Ehd) is sufficient larger enough than the square of the critical Reynolds number $Re_c$ ($Ehd>Re_c^2$) [5-7].

*Manuscript received on 20 January 2006, in final form 1October 2006.*

Yamamoto and Velkoff [3] performed numerical calculations to solve the two dimensional Navier-Stokes equations governing fluid flow with the electric field and ion distributions. Turbulent EHD analyses have been carried out to calculate the EHD flow field by solving the time-averaged Navier-Stokes equations, using $k-\varepsilon$ turbulence closure [8], RNG $k-\varepsilon$ [9] and Reynolds stress models [10]. Although the above turbulence models have previously been successfully applied in a few cases, yielding what were assumed to be reasonable results for practical ESP conditions, discussions continue on the validity of these turbulence models for ESP applications due to the isotropic assumption and/or their difficulty in showing small eddy effects, as they only appear usefulness for models with a high Reynolds number.

The model reflects a physical mechanism of EHD flow, where the ion produced by the corona discharge near to the corona wire will be transported toward the grounded wall due to

the Coulomb force. The ions provide a bulk body force to the fluid flow, resulting from the collision between the ions and neutral molecules. The body force causes the flow field to become complicated, as expressed by the product source of the space charge density and the electric field strength in the momentum equation [4].

Although there have been many experimental investigations on the particle transport in ESPs, so far only a few have directly measured the flow field inside the precipitation zone without disturbing electric field or flow. However, non intrusive optical techniques such as Laser Doppler Velocimeter (LDV) and Particle Image Velocimeter (PIV) become available for EHD-ESP flow investigations. These results show that EHD secondary flow not only generates large wake near grounded plate but also formed behind corona wire [5, 6, 7, 11, 12].

In the present study, a turbulent low/high Reynolds number model was used to investigate EHD flow, particularly the wake downstream near the corona wire. Furthermore, the mechanisms of the EHD secondary flow (ionic wind) were modeled by this selected Chen-Kim modified $k-\varepsilon$ turbulent model [13].

# 2 NUMERICAL SIMULATION

## 2.1 GENERAL SIMULATION PROCEDURE

Numerical studies were performed for a wire-plate electrostatic precipitator. The corona discharge wire, 0.9 mm in diameter, was placed in the center of the horizontal parallel plate electrodes. The lengths of the plate electrodes were 60 cm and a gap distance between two plates is 10 cm.

Steady-state two-dimensional fields were assumed to simplify the physical phenomena. The turbulent fluid flow within an ESP was calculated using the commercially available Phoenics (Version 3.5.1) CFD code [2], with a finite volume method for the time-averaged Navier-Stokes equations closed by the $k-\varepsilon$ turbulent model. A laminar model was also used to calculate the laminar flow without an EHD flow.

The ion charge density, electric field and space charge terms of the momentum equations were programmed into the user defined subroutines of the Phoenics code. The governing equations for the EHD flow field ( $u_i$ , $k$ , $\varepsilon$ ) and electrical parameters ( $E_r$ , $N_c$ ) were solved by iterative solvers, which were cycled through the equation sequence of the global iteration for coupling between the equations.

Experimental results have shown that the corona induced-turbulence is significant when $Ehd \geq \mathrm{Re}^2$ and turbulent EHD flow initiated near the corona wire [5, 6, 7, 14]. Hence, in this work, unlike the previous works based on the laminar flow model, the $k-\varepsilon$ turbulence model was chosen. In this work, the Chen-Kim modified $k-\varepsilon$ turbulent model, which has low and high Reynolds models, was chosen, since it was most effective for turbulent EHD flow near the corona wire, as it can show small eddy effects of the bulk body, such as the Von-Karman vortex in the rear flow of the wire [5, 6, 7].

## 2.2 ELECTRIC FIELD AND SPACE CHARGE DISTRIBUTION

Analytical model of Thompson [15] for a corona discharge in a coaxial wire-tube electrode geometry was used for electric field and ion density distribution. The strength of the electric field and the ion charge density were determined using Poisson's (equation 1) and the ion transport equations (equation 2) for cylindrical coordinate as follows:

$$\frac{1}{r}\frac{d(rE_r)}{dr} = -\frac{eN_c}{\varepsilon} \tag{1}$$

$$\frac{I_C}{2\pi rL} = e(U_{gr} + \mu_c E_r) N_c \tag{2}$$

where $E_r$ is the electric field, $r$ the radius, $N_c$ the number of ions, $e$ the electric elementary charge (=$1.6021892 \times 10^{-19}$ C ), $\varepsilon$ the dielectric constant (= $8.85418782 \times 10^{-12}$ F/m), $I_c$ the current, $L$ the plate depth, $U_{gr}$ the mean gas velocity and $\mu_c$ the mobility (=0.0002546 $\mathrm{cm}^2$/Vs).

By integrating equation (1), the strength of the electric field is expressed as:

$$E_r = \left( \frac{I_c}{2\pi\varepsilon\mu_c L} + \frac{{c_0}^2}{r^2} \right)^{0.5} \; ; \; E_r = -\frac{dV}{dr} \tag{3}$$

where $c_0$ is the integration constant calculated from the experimental current-voltage characteristics [15].

The ion number then yield:

$$N_c = \frac{I_c}{e2\pi rL(U_{gr} + \mu_c E_r)} \quad ; \quad \rho_{ion} = e N_c \tag{4}$$

We assumed that electric field and ion density in wire-plate ESPs can be calculated from equations (3) and (4) except electric potential at c orona wire $V = V_p$ and at grounded plate V=0.

## 2.3 EHD FLOW FIELD

For a steady-state incompressible turbulent flow, the continuity and momentum equations can be written as:

$$\frac{\partial}{\partial x_i}(\rho u_i) = 0 \tag{5}$$

$$\frac{\partial}{\partial x_i}(\rho u_i u_j) = -\frac{\partial p}{\partial x_i} + \frac{\partial}{\partial x_j}\left[ (u + u_t)\left( \frac{\partial u_i}{\partial x_j} + \frac{\partial u_j}{\partial x_i} \right) - \rho\overline{u_i' u_j'} \right] + \rho_{ion} E_i \tag{6}$$

where is the fluid mean velocity, $p$ the mean static pressure, $\mu_t$ the turbulent eddy viscosity, $u'$ the fluctuation velocity,

$\rho_{ion}$ the ion charge density and $E_i$ the strength of the electric field. The electric field strength and ion charge density are calculated from equations (3) and (4), respectively.

Using the Boussinesque eddy-viscosity hypothesis [16], the Reynolds stress tensor is expressed as:

$$-\rho\overline{u_i'u_j'} = \mu_t\left(\frac{\partial u_i}{\partial x_j}+\frac{\partial u_j}{\partial x_i}\right)-\rho k\frac{2}{3}\delta_{ij} \tag{7}$$

where $\delta_{ij}$ is the Kronecker delta.

The turbulent eddy viscosity is:

$$\mu_t = \rho C_\mu \frac{k^2}{\varepsilon} \tag{8}$$

so it is calculated from the solution of the conservation equations of the turbulent kinetic energy ($k$) and the turbulent dissipation rate ($\varepsilon$) in the standard $k-\varepsilon$ model (hereafter referred to as KE) [17].

The $k-\varepsilon$ model employs a single time scale ($k/\varepsilon$) to characterize the various dynamic processes that occur in turbulent flows. Turbulence; however, is comprised of fluctuating motions, with a spectrum of time scales, and a single-scale approach is unlikely to be adequate under all circumstances, as different turbulence interactions are associated with different parts of the spectrum. In order to remedy this deficiency in the standard model, Chen and Kim [13] proposed a modification that improves the dynamic response of the $\varepsilon$ equation. The Chen Kim modified $k-\varepsilon$ turbulent model (referred to as CK) should be proposed as both low and high Reynolds number models.

In addition, low Reynolds number models were used by Lam-Bremhorst low-Re extension to the $k-\varepsilon$ model (LB) [18], 'Yap' correction for separated flows (YAP) [19], and high Reynolds number models were used by RNG derived $k-\varepsilon$ turbulence model (RNG) [20] to compare the different models.

Turbulent intensity was calculated using the following equation:

$$I_T = \frac{\sqrt{(\overline{u'^2})}}{U_0} \tag{9}$$

The fluctuation velocity, $u'$, is calculated from the turbulent kinetic energy, as $k = 1.5u'^2$, obtained from Equation (8) with the isotropy assumption.

The dimensionless EHD number and the Reynolds number at the plate and the wire were calculated by bellow definitions [21].

The EHD numbers at the flow channel and wire are defined as follows:

$$Ehd_{FC} = \frac{I_0 L^3}{\rho_f \nu_f^2 \mu_i A} \text{ at the flow channel,}$$

$$Ehd_{CW} = \frac{I_0 d^3}{\rho_f \nu_f^2 \mu_i A} \text{ at the wire} \tag{10}$$

where $I_0$ is the reference current, $L$ the characteristic length, $P_f$ the fluid density, $\nu_f$ the fluid kinematic viscosity, $\mu_i$ the mobility, $A$ the surface area and $d$ the wire diameter.

The Reynolds numbers at the plate and wire are defined as follows:

$$\mathrm{Re}_{FC} = \frac{Lu_0}{\nu_f} \text{ based on the flow channel plate to plate}$$

$$\text{distance, } \mathrm{Re}_{CW} = \frac{d\,u_0}{\nu_f} \text{ based on the wire diameter} \tag{11}$$

where $u_0$ is the gas flow velocity. Boundary conditions based on experimental apparatus [12] used in the present study are shown in Figure 1.

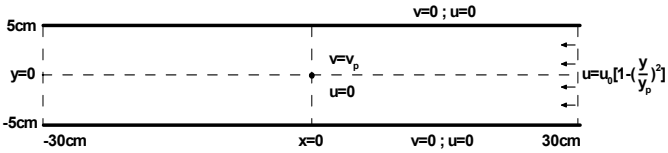


**Figure 1.** Boundary conditions used in the present calculations.

# 3 RESULTS AND DISCUSSION

## 3.1 CURRENT-VOLTAGE CHARACTERISTICS

An experimental investigation has been conducted for EHD flow study in ESP by PIV with ESP geometry as shown in Figure 1. The current-voltage characteristics observed by Podliński et al [12] for the primary flow velocity of 0.2 m/s is summarized in Table 1. The results of the PIV measurement are analyzed in term of EHD number as defined in Equation (10). These geometry and experimental values are used for the present numerical simulation.

Currents and voltages were experimentally obtained according to various gas velocity and EHD numbers by using the single wire-plate ESP test rig.

**Table 1.** Experimentally Measured Time Averaged Current-Voltage Characteristics for Mean Velocity of 0.2m/s ($Re_{CW}$=12.4, $Re_{FC}$=1377).

| Case | Voltage (kV) | Current (μA) | $Ehd_{CW}$ | $Ehd_{FC}$ |
|---|---|---|---|---|
| Laminar | 0 | 0 | 0 | 0 |
| E1 | +19.9 | 20 | $1.31\times10^6$ | $4.04\times10^2$ |
| E2 | +22.2 | 30 | $1.96\times10^6$ | $6.06\times10^2$ |
| E3 | +24.1 | 40 | $2.61\times10^6$ | $8.08\times10^2$ |
| E4 | +25.1 | 60 | $3.92\times10^6$ | $1.21\times10^3$ |
| E5 | +29.1 | 90 | $5.88\times10^6$ | $1.82\times10^3$ |

Table 1 summarizes experimentally obtained time averaged current and voltages at gas flow velocity of 0.2 m/s ($Re_{CW}$ = 12.4 at corona wire, $Re_{FC}$ = 1377 at flow channel)[12], and Table 2 summarizes experimentally obtained current and voltage ($Ehd_{CW}$ =1.31x10$^6$, $Ehd_{FC}$ =4.04x10$^2$) for various gas velocity[12].

**Table 2.** Experimentally Measured Time Averaged Current-Voltage Characteristics for Mean Velocity of 0.2m/s ($Re_{CW}$=12.4, $Re_{FC}$=1377).

| Case | Mean Velocity (m/s) | Voltage (kV) | Current (μA) | $Re_{CW}$ | $Re_{FC}$ |
|---|---|---|---|---|---|
| v0.2 | 0.2 | +19.9 | 20 | 12.4 | 1377 |
| v0.5 | 0.5 | +20.8 | 20 | 31.0 | 3441 |
| v0.8 | 0.8 | +20.3 | 20 | 49.6 | 5506 |
| v1.0 | 1.0 | +20.8 | 20 | 61.9 | 6882 |

## 3.2 EFFECT OF EHD NUMBER

Figure 2 shows the flow distribution for various applied voltages or EHD number.

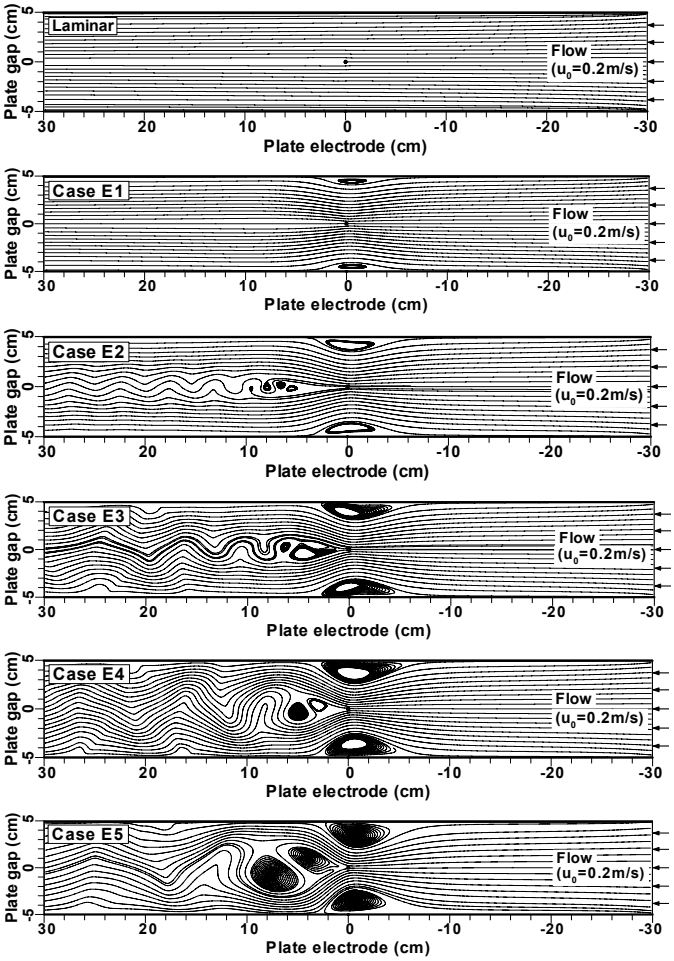


**Figure 2.** Numerical flow field results obtained corresponding to Table 1 condition.

Without an applied voltage, 0 kV, for which the EHD numbers based on the corona wire and flow channel are $Ehd_{CW}$=0 and $Ehd_{FC}$=0, respectively, "Laminar" in Figure 2 shows the usual laminar flow in the channel, as would be expected from Reynolds numbers of $Re_{CW}$ = 12.4 and $Re_{FC}$ = 1377. However, once the EHD numbers increase from $Ehd_{CW}$=1.31x10$^6$ to $Ehd_{CW}$=5.88x10$^6$, not only unsteady wakes were observed, but forward wakes were also evident. Particularly, the so called Von-Karman vortex stream was observed for $Ehd_{CW}$=1.96x10$^6$, and with increases in EHD number, such as $Ehd_{CW}$=2.61x10$^6$ through $Ehd_{CW}$=5.88x10$^6$, the downstream vortices in the channels were fully developed even at lower Reynolds number $Re_{cw}$=12.4.

As the applied voltage or EHD number increases, the greater the amount of flow interaction takes place. For $Ehd_{CW}$=5.88x10$^6$, it was clear that the gas entering the channel gradually accelerated, being deflected towards the center line of the channel due to the EHD secondary flow (i.e., ionic wind or electric wind). The level of this EHD generate turbulence was significant as there were strong interactions between the electric field, the electric charge and the gas flow. The investigation of the near-collection electrode region shows the importance of the secondary vortex flow. This means that secondary flows can have a great impact on the motion and precipitation of small particles, mainly those in the submicron range [11].

Figure 3 shows streamwise velocity profiles along the symmetry line, via the corona wire, with no applied voltage and with different applied voltages for the flow velocity, $u_0$=0.2 m/s. When Ehd=0, the velocity was only slightly changed at the outlet. However, the character of the flow changed dramatically after a voltage was applied (Ehd≠ 0), with the flow becoming turbulent and showing many different turbulent structures, as explained in Figure 2.

The gas velocity near the corona wire increases close to the front of the wire, however significantly decrease at the rear of the wire as the EHD number was increased. This was caused by the EHD flow induced by the electric body force of ions. The increasing velocity at the front wire is due to the increase in the counter flow to compensate for the vertical bulk flow, which travels in the direction of the plate electrode from the wire. Otherwise, the decrease at the rear wire is due to the streamwise velocity being decreased by the flow reversal. Particularly, in the case of Ehd>2x10$^6$, the velocities had negative values and may fluctuated due to the large flow turbulence.

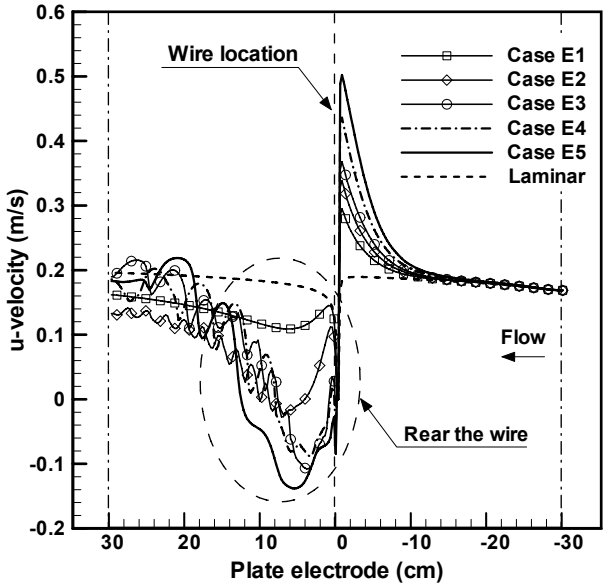


**Figure 3.** Streamwise velocities along the axis of ESPs for various EHD numbers at entrance velocity 0.2 m/s.

Figure 4 shows pressure drop of ESP and EHD induced maximum velocity to primary velocity ratio as a function of the flow channel EHD numbers ($Ehd_{FC}$) at same primary velocity 0.2 m/s ($Re_{FC}$=1377). Pressure drop, $P_{inlet}$–$P_{outlet}$, is the difference between inlet and outlet pressure, and maximum velocity ratio, $u_{max}/u_0$, is the value of maximum streamwise u-velocity divided by flow primary velocity. Figure 4 shows that pressure drop increased gradually with increasing EHD number.

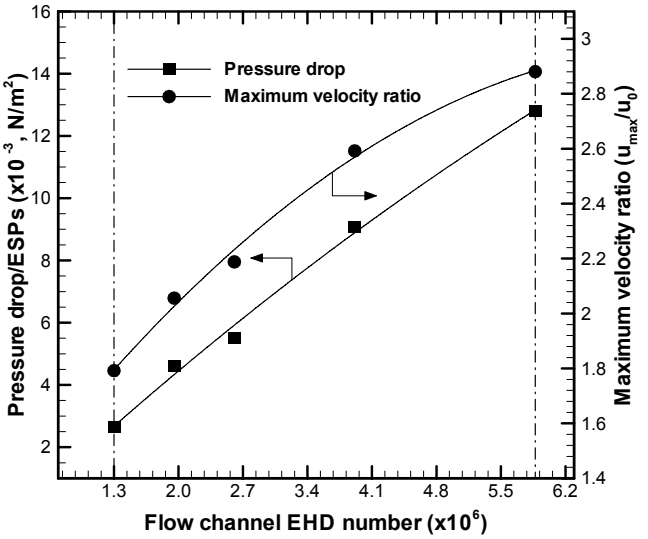


**Figure 4.** Pressure drops/ESP and EHD enhanced maximum velocity ratios as a function of EHD numbers at $Re_{FC}$=1377.

### 3.3 EFFECT OF PRIMARY REYNOLDS NUMBER

The velocity contour for different Reynolds number or gas flow velocity at inlet is shown in Figure 5 for $Ehd_{FC}$ =4.04x10$^2$.

When the gas flow velocity increase from $u_0$=0.2 m/s to $u_0$=0.8 m/s, EHD secondary flow will decrease due to large primary velocity.

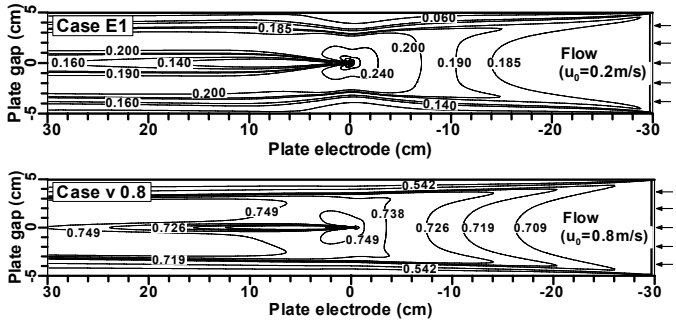


**Figure 5.** Velocity contours for a wire-plate ESPs for entrance velocity of 0.2 m/s and 0.8m/s at EHD number $Ehd_{FC}$ =4.04x10$^2$.

Figure 6 shows the u-velocity, v-velocity and turbulence intensity profiles along the symmetry line, normal to the wall of the plate electrode. As expected, the u-velocity increase with increasing in the primary flow velocity, however the v-velocity decrease, especially near the corona wire. The intensity of the turbulence increases with high flow velocity, for Re=3677, where the turbulence intensity increases significantly near wall due to the small eddy produced by friction resistance at the wall. Otherwise, for low u-flow velocity the turbulence intensity near the wire is larger than near the wall due to the bulk body force produced by the secondary flow as shown in Figure 5.

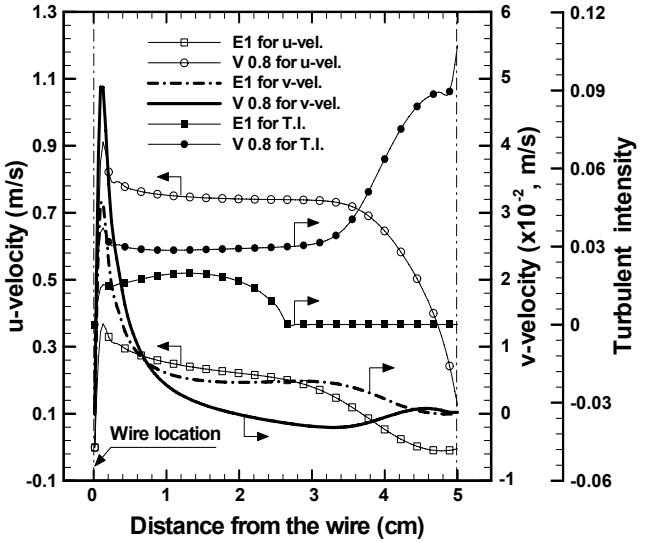


**Figure 6.** Component velocities and turbulence intensities profiles along the y-axis at x=0 (location of corona wire).

The velocity patterns near the corona wire are shown for various EHD numbers in Figure 7.

For lower EHD number flow, as shown in Figure 5, the width of the backward band flow at the rear wire was only increased by the EHD secondary flow. However, for higher EHD number the velocity vectors show a strong EHD secondary flow, which is clearly visible in the downstream regions of the corona wire, despite the low Reynolds number of the electrode ($Re_{CW}$= 12.4). The secondary flow vortices are also caused by the EHD when the applied voltage is increased. The expected life span of the ESP, particularly the corona wire, should be shortened by the vibration produced by the irregular bulk motion in the channels of a commercial ESP.

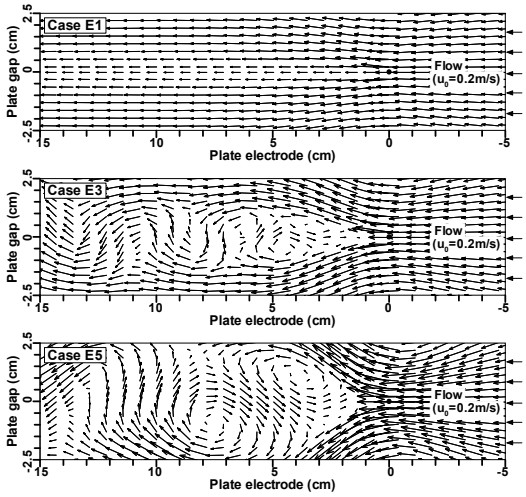


**Figure 7.** Velocity vectors of the near wire in the ESP.

### 3.4 CONCLUDING REMARKS

The numerical simulations have been used for EHD flow in wire-plate type ESPs and the following concluding remarks are obtained:

1) The flow interaction took place when a voltage was on-set. The inflow gas was gradually accelerated, and then deflected towards the center line of the channel due to the secondary flow produced by EHD forces.

2) Once EHD numbers have been increased, not only were wakes observed behind corona wires, but some forward wakes were also evident. Particularly, the so called, Von-Karman vortex stream was observed at $Ehd_{CW}=1.96x10^6$ even under low Reynolds number $Re_{cw}=12.4$. Also with the increase in the EHD number, as with $Ehd_{CW}=2.61\ x10^6$, $3.92x10^6$ and $5.88x10^6$, the vortices in the rear flow channel were fully developed.

3) Electrohydrodynamically introduced secondary flow exists not only near the dust collection electrodes, but were also observed near the corona wire. By applying a high voltage, the field velocity pattern shows a strong EHD secondary flow, which is clearly visible in the downstream regions of the corona wire, despite the low Reynolds number ($Re_{CW}$ = 12.4). Vortices are also caused by the EHD secondary flow when the applied voltage is increased. Therefore, for flow patterns near the corona wire may contaminates wires due to the EHD wake flow and part of the dust transported outside of the ESPs.

4) The EHD secondary flow may be imparting momentum to channel flow, thus increasing the pressure drop.

5) The structure of the EHD secondary flow was similar for primary inflow velocities that were sufficiently high compared to the secondary flow itself.

6) However, for the pattern above and below the corona wire, the dust particle collection may be enhanced due to the attachment of EHD wakes to the ESP collection electrode in the flow channel wall. The influence of the EHD secondary flow on the collection of the dust particle is significant at the large $Ehd/Re^2$ ratio existing in the presented ESP.

## ACKNOWLEDGMENT

Authors thank D. Borocilo, J. Podlinski and E. Dela Cruze for valuable discussions and comments. This work in supported by NSERC of Canada.

## REFERENCES

[1] F. Michel, "New Features of MIGAL solver", Proc. 9th Intern. PHOENICS User Conf., Moscow, Russia, pp. 23–27, 2002.

[2] D. B. Spalding, Software Package (Version 3.5.1), Concentration, Heat and Momentum Limited (CHAM), Located in Wimbledon, England.

[3] T. Yamamoto and H. R. Velkoff, "Electrohydrodynamics in an electrostatic precipitator", J. Fluid Mech., Vol. 108, pp. 1–12, 1981.

[4] W. J. Liang and T. H. Lin, "The Characteristics of Ionic Wind and Its Effect on Electrostatic Precipitators", Aerosol Sci. Technol., Vol. 20, pp. 330–336, 1994.

[5] J. S. Chang, D. Brocilo, K. Urashima, J. Podliński, J. Podlinski, J. Mizeraczyk, and G. Touchard, "On-Set of EHD Turbulence for Cylinder in Cross Flow Under Corona Discharges", Proc. 5th Intern. EHD workshop, Poitiers, France, pp. 26–31, 2004.

[6] P. Atten, F. M. J. McCluskey and A. C. Lahjomri, "The Electrohydrodynamic origin of turbulence in electrostatic precipitators", IEEE Trans. Ind. Appl., Vol. 23, pp.705-711, 1987.

[7] T. Yamamoto, M. Okuda and M. Okubo "Three-dimensional ionic wind and electrohydrodynamics of tuft/point corona electrostatic precipitator", IEEE Trans. Ind. Appl., Vol.39, pp.1602-1607, 2002.

[8] B. S. Choi and C. A. J. Fletcher, "Computation of particle transport in an electrostatic precipitator", J. Electrostatics, Vol. 40, No.41, pp. 413–418, 1997.

[9] S. J. Park and S. S. Kim, "Electrohydrodynamic Flow and Particle Transport Mechanism in Electrostatic Precipitators with Cavity Walls", Aerosol Sci.Tech., Vol. 33, pp. 205–221, 2000.

[10] H. J. Schemid, S. Stolz and H. Buggisch, "On the Modelling of the Electro-Hydrodynamic Flow Field in Electrostatic Precipitators Flow", Turbulence and Combustion, Vol. 68, pp. 63-89 2002.

[11] J. Mizeraczyk, M. Kocik, J. Dekowski, M. Dors, J. Podliński, T. Ohkubo, S. Kanazawa, T. Kawasaki., "Measurements of the velocity field of the flue gas flow in an electrostatic precipitator model using PIV method", Journal of Electrostatics, Vol. 51, No.52, pp. 272–277, 2001.

[12] J. Podliński, J. Dekowski, J. Mizeraczyk, D. Brocilo, and J. S. Chang, "Electrohydrodynamic gas flow in a positive polarity wire-plate electrostatic precipitator and the related dust particle collection efficiency", J. Electrostatics, Vol. 64, pp. 259–262, 2006.

[13] D. J. Monson, H. L. Seegmiller, P. K. McConnaughey, and Y. S. Chen, "Comparison of experimental with calculations using curvature-corrected zero and two-equation turbulence models for a two-dimension U-duct", AIAA-90-1484, Fluid Dynamics, Plasma Dynamics and Lasers Conference, Seattle, WA, p. 19, 1990.

[14] T. Ohkubo, S. Hamasaki, Y. Nomoto, J. S. Chang and T. Adachi, "The effect of corona wire heating on the downstream ozone concentration profiles in an air-cleaning wire-duct electrostatic precipitator", IEEE Trans. Indust. Appl. Soc., Vol. 22, pp. 542–549, 1990.

[15] J. J. Thompson, *Conduction of Electricity through Gases*, The Cambridge University Press, New York, p. 267, 1945.

[16] H. Tennekes and J. L. Lumley, *A First Course in Turbulence*, The Massachusetts Institute of Technology, p. 97, p.136, 1972.

[17] B. E. Launder and D. B. Spalding, "The numerical computation of turbulent flows", Computer Methods in Applied Mech. and Eng. Vol. 3, p. 269, 1974.

[18] V. C. Patel, W. Rodi, and G. Scheurer, "Turbulence models for near-wall and low-Reynolds-number flows: A review", AIAA J., Vol. 23, No.9, pp. 1308–1319, 1985.

[19] C. Yap, *Turbulent heat and momentum transfer in recirculating and impinging flows*, Ph.D. Thesis, Faculty of Technology, University of Manchester, 1987.

[20] V. Yakhot and S. A. Orszag, "Renormalization group analysis of turbulence", J. Sci. Comput, Vol. 1, p. 3, 1986.

[21] IEEE-DEIS-EHD Technical Committee, "Recommended International Standard For Dimensionless Parameters Used In Electrohydrodynamics," IEEE Trans. Dielectr. Electr. Insul., Vol. 10, pp.3–6, 2003.